Frontiers of Physics
https://doi.org/10.1007/s11467-018-0873-0
Front. Phys.
14(2), 23606 (2019)

RESEARCH ARTICLE

A theoretical study of step edge geometry on sapphire(0001) and its effect on ZnO nucleation

Ping Yang, Li-Xin Zhang†

School of Physics, Nankai University, Tianjin 300071, china
Corresponding author. E-mail: †*lxzhang@nankai.edu.cn*
Received July 8, 2018; accepted September 19, 2018

Step-edge-induced nucleation plays a key role in controlling the growth of novel nanostructures and low-dimensional materials. However, it is difficult to experimentally determine the step edge structures of complex metal oxides. In this work, we present a detailed theoretical study of the stability of stoichiometric steps on sapphire(0001). Based on first-principles calculations and excess charge computation by Finnis' approach, a pair of non-polar step edges are determined to be the most stable. By studying the adsorption characteristics of ZnO and combining previous works, we successfully explained how growth temperature and deposition rate affect the in-plane orientation of ZnO grown on sapphire(0001). The knowledge on the step edge structures and nucleation patterns would benefit the study on step-edge-guided nanostructure growth.

Keywords stepped sapphire surface, first-principles, excess charge, step-edge-induced nucleation

1 Introduction

C-plane sapphire is a commonly used substrate for the growth of wide-gap semiconductors such as GaN [1] and ZnO [2]. Due to the limitation of cutting machinery precision, step defects are widely present on commercial substrates [3–6]. On stepped C-plane sapphire substrate, both terrace-induced [7] and step-edge-induced [8] nucleation patterns have been reported. However, previous theoretical studies of nucleation of ZnO and GaN are limited on flat terrace [9–11]. More recently, the step edges have been revealed to play a crucial role in guiding the growth of many novel nanostructures including layered WSe_2 [12], single-wall carbon nanotubes [13] and horizontal nanowires of GaN [14] and ZnO [8, 15]. Therefore, it is of fundamental importance to study the atomic structure of step edge and the initial process of step-edge-induced nucleation. Up to now, most of experimental studies of step defects are limited to reporting on their height and orientation. The determination of edge geometry still needs the aid of theoretical simulation.

The initially polished alumina vicinal surfaces present a regular arrangement of parallel monosteps with a typical height of 0.21 nm [16, 17]. During annealing, the evolution of step morphology follows several processes including coalescence, decomposition [16], bunching, and faceting [17]. These processes lead to the gathering of several neighbour monosteps to multiple ones, whose height was detected to be $i \times 0.21$ nm (i is an integer). Most of monosteps, especially for those with very small miscut angle [17], could be preserved when the samples annealed under relative low temperature [16] for a short time [18]. Previous studies found two types of step whose edges running along either $[10\bar{1}0]$ (m-axis) or $[11\bar{2}0]$ (a-axis) directions [Fig. 1(a)]. The $[11\bar{2}0]$ steps are easy to reconstruct and form triangular faceted edges along $[1\bar{1}00]$ and $[01\bar{1}0]$, which is attributed to its weak stiffness [19]. For the $[10\bar{1}0]$ steps, only several short facets along $[11\bar{2}0]$ and $[2\bar{1}\bar{1}0]$ directions appear at "zipper-like" coalescence region [20], most of them become straight and continuous with regular intervals under appropriate annealing conditions [19]. Thus, we suggest that the $[10\bar{1}0]$ monosteps account for the vast majority on commercial C-plane sapphire substrate.

In this work, we present detailed theoretical studies on the straight stoichiometric $[10\bar{1}0]$ monosteps on C-plane sapphire. DFT calculation has been used to figure out the most stable step geometry. Moreover, we perform charge neutrality analysis to explore the correlation between step stability and its degree of polarization. Based on the proposed step geometry, we further use ZnO as an example to investigate the nucleation mechanism on both flat terrace and step edge. We reveal that nucleation sites play a decisive role in the in-plane orientation of as-grown ZnO clusters.

2 Methods

The total energy calculations were carried out using Vienna Ab initio Simulation Package (VASP) [21] based on density functional theory (DFT). Within the projec-

tor augmented wave (PAW) framework [22], the Perdew–Burke–Ernzerhof (PBE) [23] version of generalized gradient approximation (PBE-GGA) was used to describe the exchange-correlation functional. The Kohn–Sham one-electron wave functions were expanded in a plane-wave basis set with cut-off energy up to 400 eV. A symmetrized $9 \times 9 \times 5$ mesh k-points sampling was employed for geometric optimization of Al_2O_3 primitive cell. The self-consistency iteration was stopped when total energies and residual atomic forces converged to within 10^{-5} eV and 0.02 eV/Å, respectively. The calculated lattice constants ($a = 5.129$ Å) are in good agreement with experimental results ($a = 5.128$ Å) [24].

3 Theoretical modeling of steps

3.1 Step models

The Al_2O_3 hexagonal conventional unit cell is a stacking of six Al-O-Al trilayers along c-axis. For these trilayers are translationally equivalent, only three kinds of planes [labeled Al_1, O, and Al_2 in Fig. 1(b)] can be served as ideal bulk terminations on $Al_2O_3(0001)$. Both ion-scattering experiment [25] and first-principles calculations [26] proposed that $Al_2O_3(0001)$ surface has an "Al_1" termination. The height of monostep (0.21 nm) corresponds to the interplanar spacing of one trilayer ($c/6$). Therefore, we suggest that the monosteps should be a terrace transition between adjacent Al_1 terminations.

To illustrate edge geometry, we cleave a four-layer slab into two parts along $[10\bar{1}0]$ as shown in Fig. 1(c). The edge regions consisting outermost two rows of atoms on the left and right slab are labelled by I and II, respectively. The other edge geometries can be derived by changing the atomic composition in the edge regions. The four-layer slab can be viewed as a series of zigzag Al-O chains stack from left to right. After cleavage, the termination of the left slab is a line of O attached to Al of zigzag chain, while, the termination of the right slab is a line of Al attached to O of zigzag chain. The separated two slabs cannot overlap after rotation or mirror reflection operation. Therefore, we name the series of edge geometries derived from region I as type-A and those derived from region II as type-B.

In previous studies, the problem of stability of step edge was usually solved by constructing vicinal surface models and comparing their step energies [23, 28]. Figure 1(d) shows a vicinal surface with consecutive $[10\bar{1}0]$ monosteps toward $[11\bar{2}0]$ direction. The topmost Al-O-Al trilayer is identical to the left slab in Fig. 1(c), its edge belongs to type-A. The underneath trilayer can overlap the right slab in Fig. 1(c) after mirror reflection and translation operations, thus its edge belongs to type-B. Overall, the type-A and type-B monostep edges appear alternatively toward $[11\bar{2}0]$ direction. Though the structure has been proposed as described above, the long c-axis of Al_2O_3 conventional

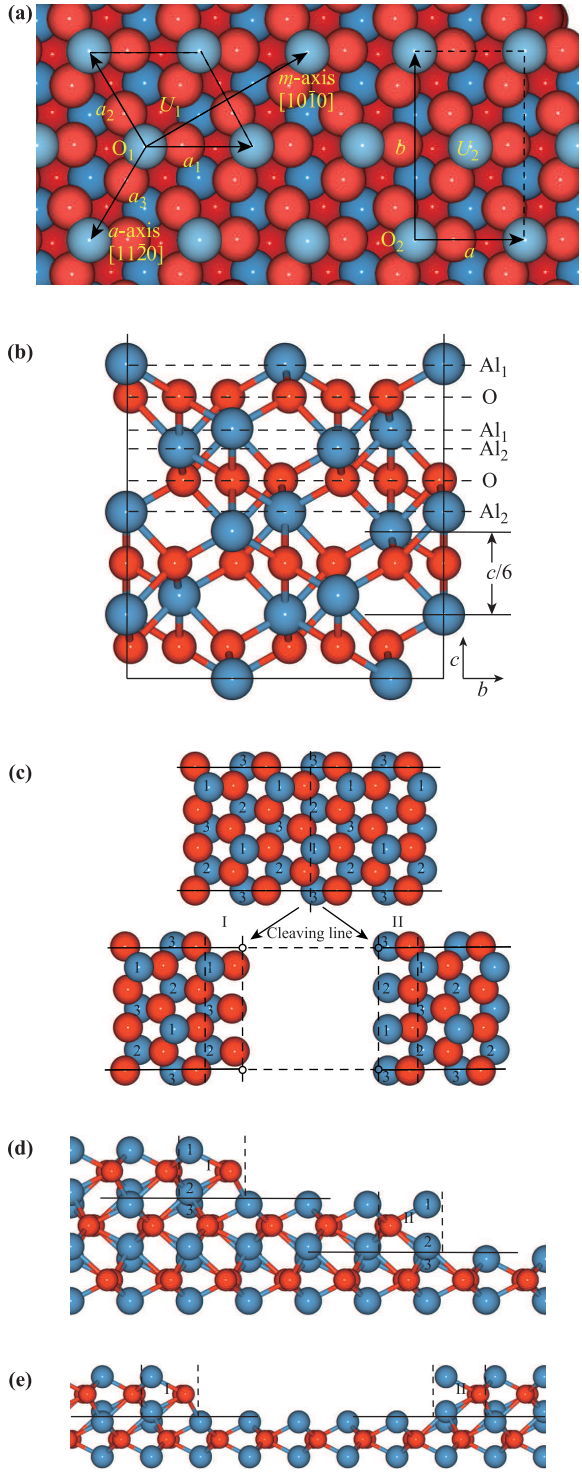

Fig. 1 **(a)** Illustration of the hexagonal conventional unit cell (U_1), orthorhombic unit cell (U_2) and two miscut directions: a-axis $[11\bar{2}0]$ and m-axis $[10\bar{1}0]$. Since the c-axis has C_3 symmetry, a axis in U_2 is identical to a_3 and the step running along b-axis is identical to that along m-axis. **(b)** Illustration of the stacking of Al_1-O-Al_2 trilayers in the orthorhombic unit cell (U_2) from side view. **(c)** Cleavage of a four-layer slab, the label 1, 2, 3 on Al are consistent with that in Fig. 1(d). **(d)** Vicinal surface model with consecutive monosteps running along $[10\bar{1}0]$ direction. **(e)** Stripe model with A-B edge pair.

unit cell results in a huge vicinal surface model size, which exceeds the range of using first-principles calculation. One practicable way is to adopt the "Stripe-E" method [29] by constructing slab models with periodic linear stripes on flat surface. As shown in Fig. 1(e), the two sides of the separated trilayer are identical to that in Fig. 1(c), the left edge belong to type-A and the right edge belong to type-B. Fortunately, on both stripe model and vicinal surface model, the type-A and type-B steps are always appear in pairs. Therefore, for any A-B edge pair configurations on real surface, we can construct their corresponding stripe models and compute total energies for judging their stability. Though many A-B edge configuration pairs can be acquired by random combination, only those stoichiometric ones are in the context of our consideration.

To construct these stripe models, we build the orthorhombic unit cell [U_2 in Fig. 1(a)] and change it to slab model by adding a vacuum width of 15 Å between the interleaved atom layers along c-axis. The surface energy of each slabs containing 3, 4, and 5 Al-O-Al trilayers is found to be about 110 meV/Å^2, which indicates that the three trilayers slab is thick enough for sufficient accurate calculations. We enlarge the slab unit consists of four Al-O-Al trilayers to the size of $6\times1\times1$ and cut five Al_2O_3 units in the middle of topmost trilayer. The length of the ditches and stripes made by cutting these atoms are more than 1 nm, which is wide enough for evading interaction between two edges.

Here, we try to figure out all candidate type-A and type-B edge pairs on the stripe model. To keep the slab stoichiometric, we change the atomic compositions by moving atoms between region I and region II in Fig. 1(e). Since the atomic compositions in two edge regions are covariant, each A-B edge pairs is named by the atomic composition in region I. (E.g., When there are one Al and two O in region I, this pair is named as Al(1)O(2)). In each slab, we set different initial atom positions in edge regions for structural optimization and select the one with minimum energy after fully relaxed. During structural optimization, the bottom two Al-O-Al trilayers are fixed to their bulk position, single Γ-point sampling is used here. The relaxed structures of all A-B edge pairs are shown in Fig. 2 and Fig. A1, the energies of each slab are listed in Table 2. The Al(2)O(1) slab (Fig. 2) has the lowest energy among these systems. From top view, the topmost Al-O-Al trilayer together with the neighbour Al1 layer follows buckled honeycomb-like arrangement. Though the Al(2) slab who exhibits zigzag boundaries on both sides is the most regular, its energy is 4.95 eV higher than that of Al(2)O(1). For Al(2)O(1) slab, type-A edge has an extra O atom (labelled O_a) attached to the zigzag boundary and type-B edge can be viewed as digging an O vacancy from the zigzag boundary.

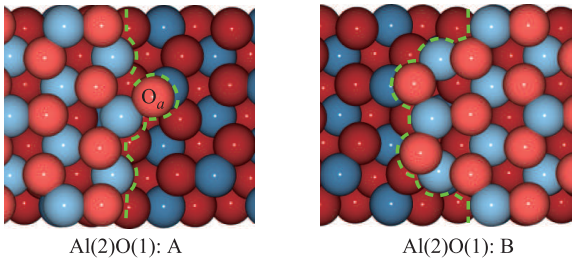

Fig. 2 Optimized structures of Al(2)O(1) edge pair. The atoms on high terrace are displayed by bright patterns and the atoms on low terrace are displayed by dark patterns. The green dashed lines mark the boundary of high terrace.

3.2 Polarity and stability

For highly ionic crystal, the stability of surfaces is believed to be strongly related to charge neutrality and dipole moment. A step edge can be regarded as a narrow slice of a surface. According to the Taker's scheme [30], the alternating rows of Al cations and O anions at the topmost Al-O-Al trilayer makes the step edges belong to either type-II non-polar or type-III polar terminations depending on the edge atomic composition. Finnis [31] has proposed an approach to calculate excess charge for quantitatively describing the degree of polarity on surface and interface. This approach has been applied to judge the stability of the step edges on Fe_3O_4(111) [32] and Fe_3O_4(100) [33]. Here, we use the same approach to calculate excess charge of the step edge models proposed above and explore the relationship between step stability and its degree of polarity.

We takes the type-A edge as an example to shows the settings for calculating excess charge in Fig. 3. All of the ions are kept to their bulk position and the "weighted linear tapered termination" is set at the O plane adjacent to edge region. The tapered volume is one Al-O-Al trilayer high, indicated by horizontal lines, and extend horizontally to the left from tapered termination. The length of tapered volume (L) is set to be only half of the basis a of U_2 in Fig. 1(a), but it is sufficient because the other atoms are identical to those in tapered volume except for a lateral displacement. Since the tapered volume contains a stoichiometric Al_2O_3 unit, the expression of positive charge excess can be simplified to $[N^+]-[N^-]$, where $[N^\pm]=\Sigma n^\pm w$, the weight $w=1-x/L$ for each atom in tapered volume and $w=1$ for each atom in the edge region [32, 33]. Based on the experiences of previous works [32, 33], it is reasonable to assign O anions a fully ionic charge of $-2e$ and assign Al cations a fully ionic charge of $+3e$. The data of each row of atoms needed in the calculation are listed in Table 1. Based on these settings, we perform excess charge calculations on these A-B step edge pair models and the results are presented in Table 2.

As can be seen in this table, the excess charge of two edges in one pair have the same numerical value with opposite signs, which is determined by symmetry. The energy of a system with higher excess charge is always higher

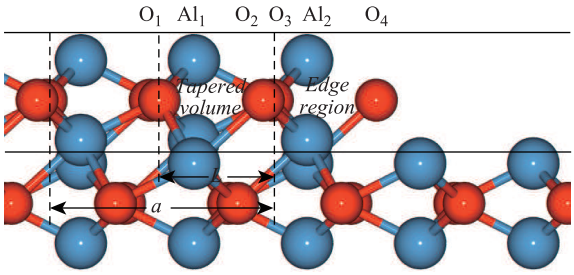

Fig. 3 Schematic of settings on the type-A step of Al(2)O(1) model for computing charge excess by Finnis approach. The name of each row in tapered volume and edge region are labelled above.

Table 1 The ionic charge ($n^{\pm}$) and weight (w) of each row of atoms of Fig. 3 are listed here.

Atom row	O_1	Al_1	O_2	O_3	Al_2	O_4
w	0	0.305	0.92	1	1	1
$n^+(e)$	0	6	4.68	0	6	0
$n^-(e)$	−4	0	4.10	−4	0	−2
$n^+w(e)$	0	1.83	3.66	0	6	0
$n^-w(e)$	0	0	0	−4	0	−2

Table 2 Excess charge and energies of each step edge pair. $EC_{A(B)}$ is excess charge of type-A(B) edge, E_0 is the energy of Al(2)O(1) step model.

Step edge pair	$EC_A(e)$	$EC_B(e)$	$E - E_0$(eV)
Al(2)O(1)	0	0	0
Al(3)O(2)	+1	−1	3.66
Al(1)	−1	1	4.10
Al(2)O(2)	−2	2	4.68
Al(2)	+2	−2	4.95
Al(1)O(1)	−3	3	6.59
Al(3)O(1)	+3	−3	7.36
Al(2)O(3)	−4	+4	10.81
Al(1)O(2)	−5	5	13.52

than those with lower excess charge. Between systems with the same excess charge, there is still a significant energy difference. For the lowest energy system [Al(2)O(1)], the excess charge on both two edges are zero, which means the atomic composition in edge regions properly cancels the inner dipole moments. As can be seen from Fig. A1, some edges with large excess charge exhibit obvious reconstruction. For example, an O atom detach from the Al(1)O(2)-A edge and a Zn atom detach from the Al(3)O(1)-A edge, which results in a decrease of polarity on edges. These results reveal that the degree of polarity is the main factor determining the stability of these step edges, other factors such as the coordination situation of edge atoms are also non-negligible. We suggest that the non-polar Al(2)O(1) edge pair accounts for the vast majority of the steps appear on Al_2O_3(0001) for its relatively low energy.

4 Nucleation and in-plane orientation

The in-plane orientation of ZnO films grown on sapphire(0001) was reported to be either ZnO[10$\bar{1}$0]‖sapphire[10$\bar{1}$0] [34] or ZnO[10$\bar{1}$0]‖sapphire[11$\bar{2}$0] [35]. According to the orientation between hexagon lattice of ZnO and Al_2O_3, the former is named as "30° twisted" and the latter is named as "aligned in-plane". On sapphire(0001) substrate with monosteps, the preferential in-plane orientation was reported to be "30° twisted" at low temperature and high deposition rate. The "aligned in-plane" orientation become dominant with the increase of growth temperature or with the decrease of deposition rate [6]. We find that in the case of WSe_2 grown on stepped sapphire(0001) and graphene grown on stepped Ir(111), high deposition temperature can promote species nucleate at step edges [12, 36]. Shiota *et al.* [37] explains that high temperature help to increase the activity of deposition species. When the diffusion length exceeds the width of terrace, more atoms can reach the step edge and be trapped. In addition to raising growth temperature, people also choose low deposition rates to promote step-edge-induced nucleation [8, 38]. One reasonable explanation is that low deposition rate reduce the density of species and avoid them attach each other and nucleate on terrace before diffusing to the edge. Based on the discussion above, the "30° twisted" ZnO would be initiated from terrace-induced nucleation and the "aligned in-plane" ZnO would be initiated from step-edge-induced nucleation.

In order to confirm this hypothesis, the adsorption characteristics of ZnO on flat terrace and step edges should be studied in detail. We compare the formation energies of stoichiometric Zn_nO_n clusters to figure out their most stable adsorption geometry. The formation energy of each Zn_1O_1 molecules is defined as

$$E_{form} = (E_{tot} - E_{sub} - n \times E_{\mathrm{ZnO}[bulk]})/n,$$

where E_{tot} is the energy of the adsorption system and E_{sub} is the energy of substrate, the energy of a Zn_1O_1 molecule in ZnO bulk phase ($E_{\mathrm{ZnO}[bulk]}$) is taken as the energy reference, n is the number of adsorbed Zn_1O_1 molecules.

An optimized $3 \times 3 \times 1$ Al_2O_3 slab consist of four Al-O-Al trilayers separated by 15 Åvacuum layer was chosen as the substrate for investigating terrace-induced nucleation. All optimized structures of Zn_nO_n clusters are shown in Fig. 4(a) and Fig. A2. Previous study has reported that the isolated O atom is the most stable when attaching to Al1 atom and the binding of Zn on the whole substrate is very weak, which makes it easy to diffuse [9]. The optimized geometry of Zn_1O_1 molecule accords with these

properties. Two Zn_1O_1 molecules with O atoms attached to neighbour Al1 atoms can form a Zn-O-Zn-O chain. By changing the position of the next Zn_1O_1 molecule attached to this chain, we construct different configurations of Zn_3O_3 cluster including the straight chain, bending chain, Y-shape chain and circle. The straight and Y-shape chains break into two parts after optimization. Formation energy of the circle is 0.42 eV smaller than that of bending chain. These results indicate that the adsorbed ZnO prefer to form a circle rather than any kind of chain at the initial stage of nucleation on flat terrace. The circle can be regarded as a small contraction from a hexagon in wurtzite ZnO with the orientation as shown by the dashed line circle in Fig. 4(a), who coincides with the hexagon lattice of Al_2O_3 after 30° rotation. It is well known that the film orientation is generally determined at the initial stage of the epitaxy. Thus, the in-plane orientation of ZnO initiate from terrace-induced nucleation should be "30° twisted".

The Al(2)O(1) slab is used as the substrate for investigating step-edge-induced nucleation. The candidate adsorption configurations on Type-A edge are shown in Fig. A3 and those on type-B edge are shown in Fig. 4(b) and Fig. A4. On both type-A and type-B edges, the Zn_1O_1 molecule with O attach to the Al atom on flat terrace is the most stable. On type-A edge, the Zn_2O_2 bending chain is still much more stable than the zigzag chain. The formation energies of clusters with O atoms attached to edge Al atoms are even much higher than those adsorbed on flat terrace. These indicate that Al atoms on type-A edge have little effect on ZnO nucleation. Only the O_a atom shows relatively strong interaction with Zn, however, its effect on nucleation pattern is still unclear. On type-B edge, the Zn_2O_2 chain is most stable when it forms a Zn-Al-O hexagon together with the edge atoms, which is marked by dashed lines in Fig. 4(b). This hexagon can be regarded as an extension of the honeycomb-like lattice of high terrace. The Zn_2O_3 cluster added to the left of the Zn_2O_2(a) system, shown in Fig. 4(c), also exhibits a hexagon arrangement with the same orientation. Thus, ZnO epitaxy from type-B edge could keep the hexagonal lattice arrangement during outward extension, which determines the in-plane orientation to be "aligned in-plane". The formation energies of the most stable Zn_1O_1 and Zn_2O_2 configurations are much lower than those on type-A edge and the circle on flat terrace. These results means that type-B edge is the most active site for ZnO adsorption which is benefit to step-edge-induced nucleation under high temperature. The nucleation characteristics on both flat terrace and type-B edge derived by first-principles calculation accord well with experimental observations.

Nucleation orientation control is an important step to realize high quality single crystal growth and thus receiving widespread attention. Besides ZnO, previous studies have also found the effect of sapphire substrates on the orientation of several 2D material. For example, MoS_2 nucleate on terrace exhibit random orientation [39], while

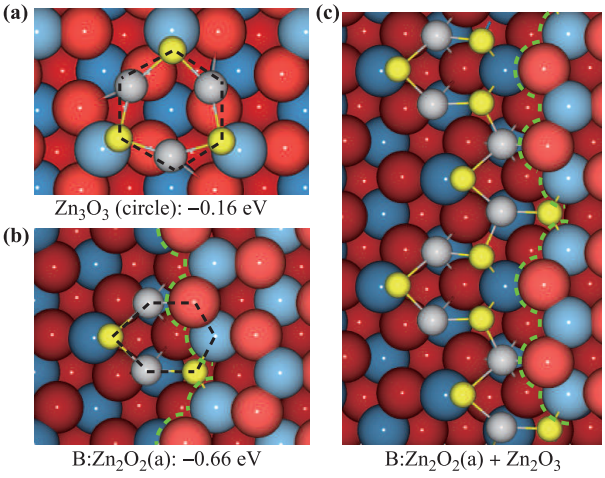

Fig. 4 The key adsorption configurations of Zn_nO_n cluster. **(a)** Zn_3O_3 circle on flat terrace. **(b)** Zn_2O_2 cluster with minimum adsorption energy on type-B edge. **(c)** Illustration of extension of ZnO hexagon from type-B edge. Grey balls are Zn atoms, yellow balls are added O atoms. The formation energies of each Zn_1O_1 molecule are listed below.

step-edge-induced nucleation can promote aligned growth of WSe_2 [12]. Since this kind of 2D materials also have hexagonal lattice, we believe that the mechanism of edge-induced ZnO nucleation may also be applicable to them. The more general mechanism of hexagonal materials nucleate on sapphire step is worth to be revealed by future studies.

5 Conclusion

In summary, we have studied the steps on C-plane sapphire by computing both energies and excess charge of various bulk truncated monostep models. As a highly ionic crystal, the degree of local polarization on step edge is strongly correlated to its stability. The most stable step edge geometry is determined to be the non-polar Al(2)O(1) edge pair. We suggest that when studying step structures on other complex polar crystal, we can also rule out the systems with high degree of polarity by comparing excess charge. By studying the nucleation pattern of ZnO, we convince that the "30° twisted" and "aligned in-plane" orientation patterns are initiated by flat terrace-induced and type-B edge-induced nucleation, respectively. These findings are helpful in simplifying the study of the stability of metal oxide steps and deepening the understanding of step-edge-induced nucleation mechanism on C-plane sapphire substrate.

Acknowledgements This work was supported by the National Natural Science Foundation of China under Grant Nos. 11274179 and 11574157 and the National 973 Projects of China under Grant No. 2012CB921900.

Appendix A

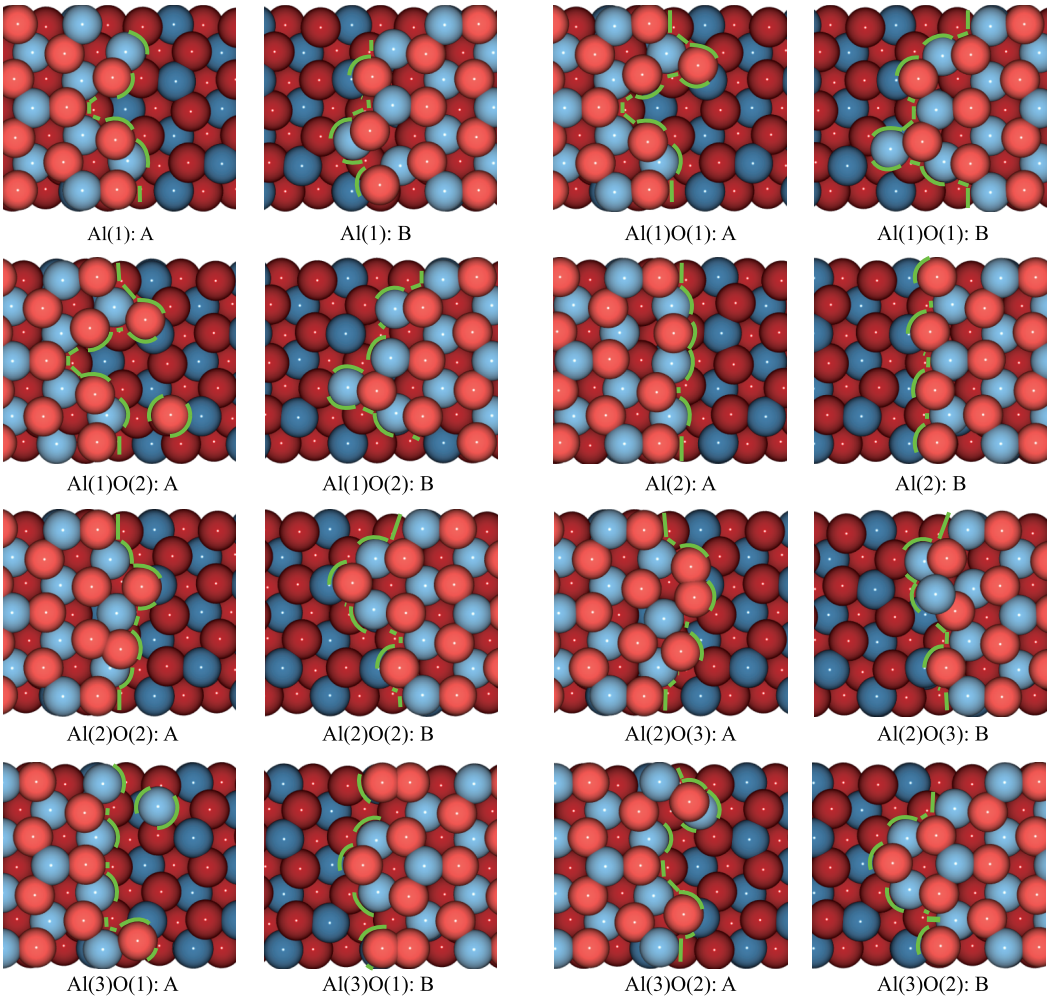

Fig. A1 Optimized structures of 8 pairs of candidate edge pairs other than Al(2)O(1).

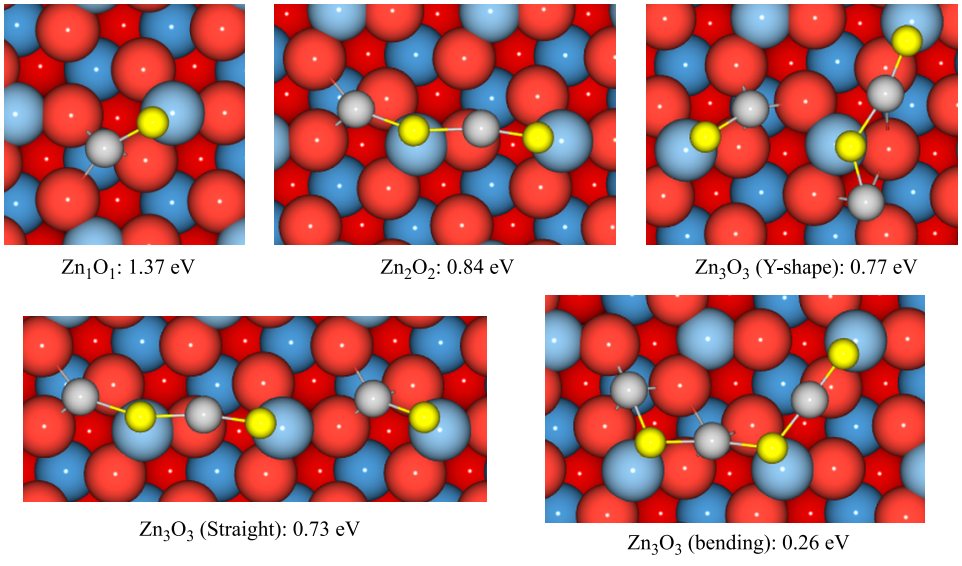

Fig. A2 The adsorption configurations of Zn_nO_n clusters (other than Zn_3O_3 circle) on flat terrace and their corresponding adsorption energies.

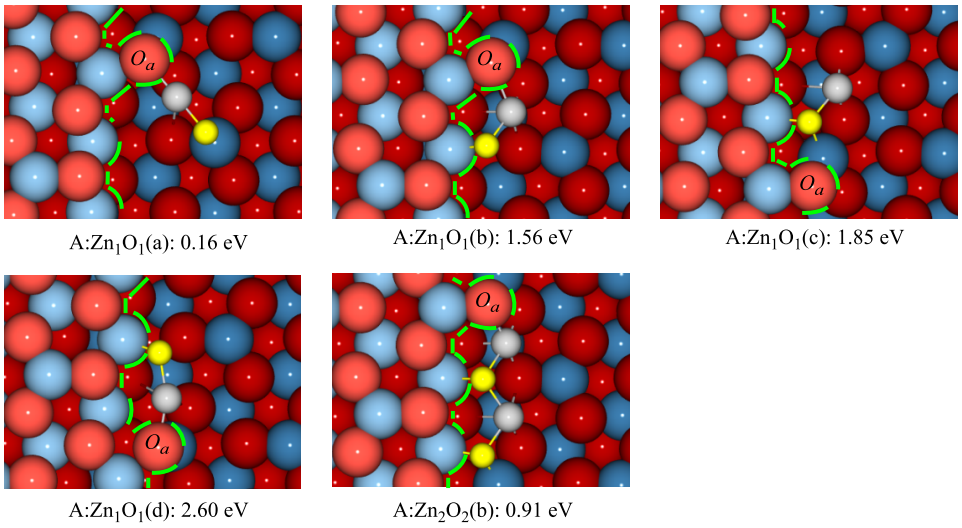

Fig. A3 The adsorption configurations of Zn_nO_n clusters on Type-A edge and their corresponding adsorption energies.

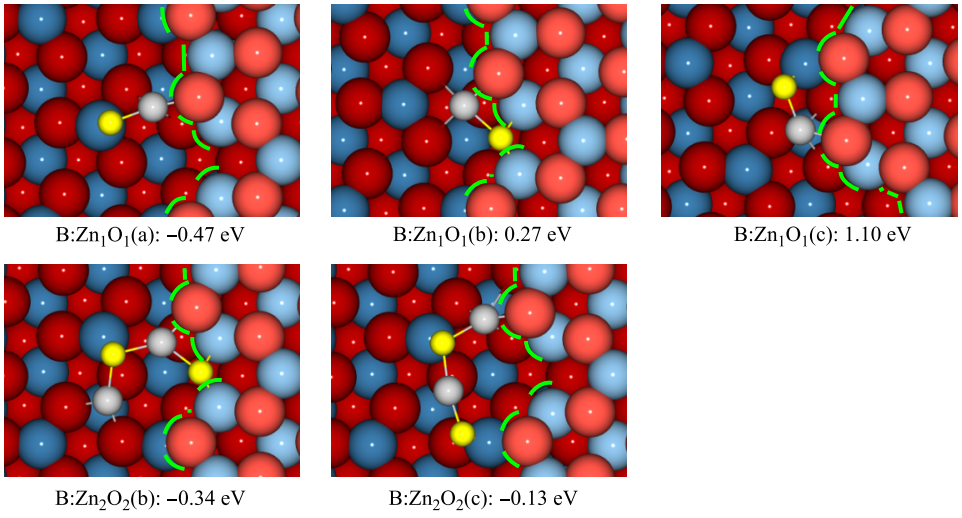

Fig. A4 The adsorption configurations of Zn_nO_n clusters [other than Zn_2O_2(a)] on Type-B edge and their corresponding adsorption energies.

References

1. I. Akasaki, Nobel Lecture: Fascinated journeys into blue light, *Rev. Mod. Phys.* 87(4), 1119 (2015)
2. U. Özgür, Y. I. Alivov, C. Liu, A. Teke, M. A. Reshchikov, S. Doğan, V. Avrutin, S. J. Cho, and H. Morkoç, A comprehensive review of ZnO materials and devices, *J. Appl. Phys.* 98(4), 041301 (2005)
3. M. Yoshimoto, T. Maeda, T. Ohnishi, H. Koinuma, O. Ishiyama, M. Shinohara, M. Kubo, R. Miura, and A. Miyamoto, Atomic-scale formation of ultrasmooth surfaces on sapphire substrates for high-quality thin-film fabrication, *Appl. Phys. Lett.* 67(18), 2615 (1995)
4. C. C. Kim, J. H. Je, P. Ruterana, F. Degave, G. Nouet, M. S. Yi, D. Y. Noh, and Y. Hwu, Microstructures of GaN islands on a stepped sapphire surface, *J. Appl. Phys.* 91(7), 4233 (2002)
5. C. Munuera, J. Zúñiga-Pérez, J. F. Rommeluere, V. Sallet, R. Triboulet, F. Soria, V. Muñoz-Sanjosé, and C. Ocal, Morphology of ZnO grown by MOCVD on sapphire substrates, *J. Cryst. Growth* 264(1–3), 70 (2004)
6. I. Ohkubo, A. Ohtomo, T. Ohnishi, Y. Mastumoto, H. Koinuma, and M. Kawasaki, In-plane and polar orientations of ZnO thin films grown on atomically flat sapphire, *Surf. Sci.* 443(1–2), L1043 (1999)
7. D. Dumcenco, D. Ovchinnikov, K. Marinov, P. Lazić, M. Gibertini, N. Marzari, O. L. Sanchez, Y. C. Kung, D. Krasnozhon, M. W. Chen, S. Bertolazzi, P. Gillet, A. Fontcuberta i Morral, A. Radenovic, and A. Kis, Large-area epitaxial monolayer MoS_2, *ACS Nano* 9(4), 4611 (2015)
8. J. Y. Son, S. J. Lim, J. H. Cho, W. K. Seong, and H. Kim, Synthesis of horizontally aligned ZnO nanowires localized at terrace edges and application for high sensitivity gas sensor, *Appl. Phys. Lett.* 93(5), 053109 (2008)

9. K. Fujiwara, A. Ishii, T. Ebisuzaki, T. Abe, and K. Ando, Theoretical investigation on the structural properties of ZnO grown on sapphire, *e-J. Surf. Sci. Nanotech.* 4, 544 (2006)
10. C. Yang, Y. R. Li, and J. S. Li, *Ab initio* total energy study of ZnO adsorption on a sapphire (0001) surface, *Phys. Rev. B* 70(4), 045413 (2004)
11. J. Ohta, H. Fujioka, M. Oshima, K. Fujiwara, and A. Ishii, Experimental and theoretical investigation on the structural properties of GaN grown on sapphire, *Appl. Phys. Lett.* 83(15), 3075 (2003)
12. L. Chen, B. Liu, M. Ge, Y. Ma, A. N. Abbas, and C. Zhou, Step-edge-guided nucleation and growth of aligned WSe_2 on sapphire via a layer-over-layer growth mode, *ACS Nano* 9(8), 8368 (2015)
13. A. Ismach, L. Segev, E. Wachtel, and E. Joselevich, Atomic-step-templated formation of single wall carbon nanotube patterns, *Angew. Chem. Int. Ed.* 43(45), 6140 (2004)
14. D. Tsivion, M. Schvartzman, R. Popovitz-Biro, P. von Huth, and E. Joselevich, Guided growth of millimeter-long horizontal nanowires with controlled orientations, *Science* 333(6045), 1003 (2011)
15. D. Tsivion, M. Schvartzman, R. Popovitz-Biro, and E. Joselevich, Guided growth of horizontal ZnO nanowires with controlled orientations on flat and faceted sapphire surfaces, *ACS Nano* 6(7), 6433 (2012)
16. L. Pham Van, O. Kurnosikov, and J. Cousty, Evolution of steps on vicinal (0001) surfaces of α-alumina, *Surf. Sci.* 411(3), 263 (1998)
17. O. Kurnosikov, L. Pham Van, and J. Cousty, High-temperature transformation of vicinal (0001) Al_2O_3-α surfaces: An AFM study, *Surf. Interface Anal.* 29(9), 608 (2000)
18. F. Cuccureddu, S. Murphy, I. V. Shvets, M. Porcu, H. W. Zandbergen, N. S. Sidorov, and S. I. Bozhko, Surface morphology of c-plane sapphire (a-alumina) produced by high temperature anneal, *Surf. Sci.* 604(15–16), 1294 (2010)
19. Y. Shiratsuchi, M. Yamamoto, and Y. Kamada, Surface structure of self-organized sapphire(0001) substrates with various inclined angles, *Jpn. J. Appl. Phys.* 41(Part 1, No. 9), 5719 (2002)
20. B. Qi, B. Agnarsson, S. Ólafsson, H. P. Gíslason, and M. Göthelid, Room temperature deposition of self-assembled Al nanoclusters on stepped sapphire(0001) surface and subsequent nitridation, *Thin Solid Films* 520(1), 64 (2011)
21. G. Kresse and J. Furthmüller, Efficiency of ab-initio total energy calculations for metals and semiconductors using a plane-wave basis set, *Comput. Mater. Sci.* 6(1), 15 (1996)
22. P. E. Blöchl, Projector augmented-wave method, *Phys. Rev. B* 50(24), 17953 (1994)
23. J. P. Perdew, K. Burke, and M. Ernzerhof, Generalized gradient approximation made simple, *Phys. Rev. Lett.* 77(18), 3865 (1996)
24. S. D. Mo and W. Y. Ching, Electronic and optical properties of θ-Al_2O_3 and comparison to α-Al_2O_3, *Phys. Rev. B* 57(24), 15219 (1998)
25. J. Ahn and J. W. Rabalais, Composition and structure of the $Al_2O_3\{0001\}$-(1×1) surface, *Surf. Sci.* 388(1–3), 121 (1997)
26. T. Kurita, K. Uchida, and A. Oshiyama, Atomic and electronic structures of α-Al_2O_3 surfaces, *Phys. Rev. B* 82(15), 155319 (2010)
27. J. Stausholm-Møller, H. H. Kristoffersen, U. Martinez, and B. Hammer, A density functional theory study of atomic steps on stoichiometric rutile TiO_2 (110), *J. Chem. Phys.* 139(23), 234704 (2013)
28. B. Lee and D. R. Trinkle, Energetics of rutile TiO_2 vicinal surfaces with $\langle 001 \rangle$ steps from the energy density method, *J. Phys. Chem. C* 119(32), 18203 (2015)
29. S. M. Kozlov, F. Viñes, N. Nilius, S. Shaikhutdinov, and K. M. Neyman, Absolute surface step energies: Accurate theoretical methods applied to ceria nanoislands, *J. Phys. Chem. Lett.* 3(15), 1956 (2012)
30. P. W. Tasker, The stability of ionic crystal surfaces, *J. Phys. C Solid State Phys.* 12(22), 4977 (1979)
31. S. Köstlmeier, C. Elsässer, B. Meyer, and M. W. Finnis, A density functional study of interactions at the metal–ceramic interfaces $Al/MgAl_2O_4$ and $Ag/MgAl_2O_4$, *Phys. Status Solidi (a)* 166(1), 417(1998)
32. V. E. Henrich and S. K. Shaikhutdinov, Atomic geometry of steps on metal-oxide single crystals, *Surf. Sci.* 574(2–3), 306 (2005)
33. H. Q. Wang, E. I. Altman, and V. E. Henrich, Steps on $Fe_3O_4(100)$: STM measurements and theoretical calculations, *Phys. Rev. B* 73(23), 235418 (2006)
34. R. D. Vispute, V. Talyansky, Z. Trajanovic, S. Choopun, M. Downes, R. P. Sharma, T. Venkatesan, M. C. Woods, R. T. Lareau, K. A. Jones, and A. A. Iliadis, High quality crystalline ZnO buffer layers on sapphire(001) by pulsed laser deposition for III–V nitrides, *Appl. Phys. Lett.* 70(20), 2735 (1997)
35. Y. Chen, D. M. Bagnall, H. J. Koh, K. T. Park, K. Hiraga, Z. Zhu, and T. Yao, Plasma assisted molecular beam epitaxy of ZnO on c-plane sapphire: Growth and characterization, *J. Appl. Phys.* 84(7), 3912 (1998)
36. J. Coraux, A. T N'Diaye, M. Engler, C. Busse, D. Wall, N. Buckanie, F.-J. M. zu Heringdorf, R. van Gastel, B. Poelsema, and T. Michely, Growth of graphene on Ir(111), *New J. Phys.* 11(2), 023006 (2009)
37. T. Shiota, H. Ito, N. Wakiya, J. Cross, O. Sakurai, and K. Shinozaki, Effect of step edges on the growth of Pt thin films on oxide single-crystal substrates, *J. Ceram. Soc. Jpn.* 121(1411), 278 (2013)
38. B. J. Murray, E. C. Walter, and R. M. Penner, Amine vapor sensing with silver mesowires, *Nano Lett.* 4(4), 665 (2004)
39. D. Dumcenco, D. Ovchinnikov, K. Marinov, P. Lazić, M. Gibertini, N. Marzari, O. L. Sanchez, Y. C. Kung, D. Krasnozhon, M. W. Chen, S. Bertolazzi, P. Gillet, A. Fontcuberta i Morral, A. Radenovic, and A. Kis, Large-area epitaxial monolayer MoS_2, *ACS Nano* 9(4), 4611 (2015)